

Effects of Hot Spinning and Heat Treatment on the Microstructure, Texture, and Mechanical Properties of A356 Wheel Hubs



CHANGQING HUANG and JIAXING LIU

The effects of hot spinning and heat treatment on the microstructure, texture, and mechanical properties of A356 wheel hubs were studied. The results of the microstructure investigation show that the as-cast microstructure was broken and elongated after spinning, but the microstructure in the inner layer was not substantially streamlined. The results obtained for the eutectic Si particles reveal that they were partially cracked under the action of the spinning stress, resulting in a slight decrease in size. The spheroidization effect of heat treatment on the eutectic Si particles was significant. The results of texture research show that the original as-cast texture disappeared after spinning, and the subsequent heat treatment had an influence on the texture transformation. The distribution of the misorientation angle changed after hot spinning and heat treatment. The hardness results show that the hardness decreased slightly by spinning but increased with the subsequent heat treatment. Both spinning and heat treatment could improve the tensile strength, but the tensile strength of the inner layer was lower than that of the outer layer. The effect of the developed textures on the yield strength was explored by a comparison study using the Schmid Factor.

<https://doi.org/10.1007/s11661-019-05476-7>

© The Minerals, Metals & Materials Society and ASM International 2019

I. INTRODUCTION

A356 aluminum alloy is a representative Al-Si-Mg alloy with excellent castability, such as good fluidity, low linear shrinkage, and a low probability of thermal cracking, which can be utilized for thin-wall and complex part casting. It can obtain high-specific strength, good plasticity, and excellent impact toughness by heat treatment.^[1-3] In addition, A356 aluminum alloy is commonly employed in the manufacturing of automobile wheel hubs and other parts because of its good welding properties, anti-corrosion performance and anti-fatigue performance.^[4] The manufacturing methods for aluminum alloy wheel hubs usually include casting, forging, and cast-spinning, among which the cast-spinning method has been extensively employed for its high material utilization rate, high productivity, and flexibility for the production of wheel hubs of different

specifications.^[5] In general, heat treatment is performed after spinning to improve the strength (generally by T6 temper; solution treatment and aging).

Due to the significant influence and complex action mechanism of the plastic deformation and heat treatment on the microstructure and properties of material, there are continuous studies dedicated to this field. Several studies concerning A356 α -Al primary dendrites, secondary dendritic arm spacing, eutectic Si, secondary phases (β -Al₅Fe₂Si and π -Al₈FeMg₃Si₆) and fracture behavior have been published to characterize the evolution of the microstructure and mechanical properties of A356 aluminum alloy during the hot spinning process under the conditions of different reduction ratios.^[6-8] Cheng *et al.*^[9] investigated the influence of spinning on the wear and corrosion performance of A356 alloy, and the results showed that spinning deformation was beneficial for reducing wear rate and corrosion current density. There are a series of reports about the heat treatment of A356 aluminum alloy, which focused on the effects of heat treatment (T4, T5, and T6 tempers) on the microstructure, tensile performance, fracture mechanism, hardness, and damping ratio.^[10-14] However, published research on the spinning of the A356 alloy has not studied the inhomogeneity of deformation in the material during the spinning process, although this largely impacts the material performance. In addition, most of the studies on the heat treatment of A356 focused on the as-cast material. The variation of the

CHANGQING HUANG is with the School of Mechanical and Electrical Engineering, State Key Laboratory of High-performance Complicated Manufacturing and Light Alloy Research Institute, Central South University, Changsha 410083, China. Contact e-mail: huangcq64@hotmail.com JIAXING LIU is with the School of Mechanical and Electrical Engineering and State Key Laboratory of High-performance Complicated Manufacturing, Central South University, Changsha 410083, China.

Manuscript submitted June 13, 2019.

Article published online November 11, 2019

microstructure and performance of the target material from the casting state to the spinning state, and from the spinning state to the heat treatment state have not been systematically studied.

Texture is an important parameter for determining the properties and deformation mechanism of material, and proper control substantially enhances the properties of the material. Howeyze *et al.*^[15] explored the effects of deformation routes on the texture and tensile properties of AA5052 aluminum alloy, and found that the texture developed in the pressed sample had a softening effect on the material. It was reported that the texture of the A356-T6 as-cast alloy developed in the process of friction stir welding with a high-rotational speed of the friction head could further improve the fatigue strength compared with the weak texture that occurred under a low-rotational speed.^[16] Zhao *et al.*^[17] reported that, when tensile testing for polycrystalline magnesium alloys with specifically oriented columnar grain structures (crystal growth direction $\langle 01\bar{1}0 \rangle$) was carried out at 350 °C, the elongation could reach 42 pct. They assumed that the high ductility was associated with the high-orientation consistency between the adjoining grains. However, the texture evolution in the spinning and subsequent heat treatment process of the A356 aluminum alloy has not been investigated, although this understanding is critical for the control and enhancement of the performance of the cast-spinning wheel hub.

This work aims to study and analyze the effects of hot spinning and subsequent heat treatment on the microstructure, texture, and mechanical properties of A356 wheel hubs, depending on the processing changes. In particular, the microstructure and eutectic Si in different areas of the spinning deformed (SD) and heat-treated (HT) samples are first discussed. Next, the texture evolution and the variation of misorientation angle in different areas of the SD and HT samples are investigated. Finally, the variation of the mechanical properties and the effect of texture types on the yield strength of the studied material are discussed.

II. MATERIALS AND EXPERIMENTS

A. Hot Spinning Experiment

The A356 aluminum alloy wheel hub blank was made by low-pressure die casting (LPDC), and its chemical composition is illustrated in Table I. The hot spinning experiment was carried out on a vertical spinning machine used for aluminum alloy wheel hubs. The spinning diagram is shown in Figure 1(a). The blank was preheated to 360 °C in the heat treatment furnace before the spinning processing and then placed on the spinning machine. The upper die and mandrel were heated to 200 °C, and the three rollers were heated to 100 °C. The spindle speed was set at 500 r.min⁻¹, and the feed rate was set at 1 mm.r⁻¹. The section taken from the wheel rim of the deformed sample is shown in Figure 1(b).

B. Heat Treatment

The SD samples were submitted to T6 heat treatment after hot spinning, which consisted of solution treatment at 545 ± 5 °C for 280 minutes and subsequent artificial aging at 154 ± 5 °C for 180 minutes. Finally, they were cooled to the ambient temperature in the air.

C. Microstructure Analysis

An Olympus DSX500 optical microscope (OM) was used to observe and analyze the microstructure. The longitudinal section samples were taken from the middle rim of SD and HT hubs, and the as-cast samples were directly taken from the LPDC blank. The metallographic sample preparation process started with grinding the samples. Rough grinding occurred first, followed by polishing with P240-320-600-1200-2000 SiC sandpapers, and then fine grinding was performed. Lastly, the samples were etched by a hydrofluoric acid solution, cleaned with absolute ethyl alcohol and dried. A Phenom scanning electron microscope (SEM) was employed to observe the morphology of the eutectic Si particles. The SEM sample preparation was similar to the metallographic sample preparation, except that the etch agent was Keller's etch. Image ProPlus Software was used to measure the mean diameter (MD) and roundness (R) of the eutectic Si for quantitative analysis. Measurements were performed depending on the ASTM E112 standard, and 50 measurements each optical field were carried out on five fields. MD and R are defined as follows^[12]:

$$MD = \frac{\sum_i^n D_i}{n} \quad [1]$$

where D_i represents the length of transverse lines passing across eutectic Si's centroid, and each length of D_i was measured at an interval of 2 deg; n is the number of transverse lines.

$$R = \frac{p^2}{4\pi A} \quad [2]$$

where p , A are the perimeter and area of a particle, respectively.

D. Electron-Backscattered Diffraction Experiments

To study the texture evolution of the A356 aluminum alloy wheel hub after hot spinning and T6 treatment, electron-backscattered diffraction (EBSD) experiments were conducted to observe and analyze the grain orientation of the as-cast, SD, and HT samples. The EBSD sample preparation process started with the same grinding as the OM sample preparation process. Electrolytic polishing occurred next with an electrolyte solution comprised of 10 ml of perchloric acid and 90 ml of anhydrous ethanol. The cathode was stainless steel, and the etching process occurred at room temperature and 24 V for 30 seconds.

Table I. Chemical Composition of A356 Aluminum Alloy

Elements	Si	Mg	Fe	Cu	Zn	Mn	Ti	Res.	Al
Wt Pct	6.88	0.30	0.06	0.03	0.03	0.03	0.2	0.13	bal.

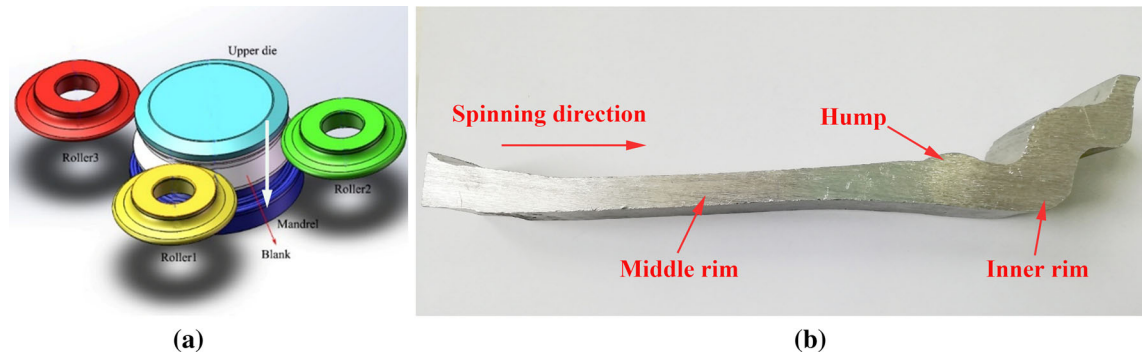


Fig. 1—(a) Schematic diagram of spinning, (b) section taken from the deformed sample.

Quantitative analysis of texture was conducted by calculating the orientation distribution functions (ODFs), misorientation angle, and Schmid Factor from the EBSD data using TSL-OIM software.

E. Mechanical Properties Tests

The tensile samples were taken along the axial direction of the inner and outer layers of the rim in the hubs with different processing states, and the as-cast tensile samples were machined from the LPDC blank. The room temperature tensile tests were conducted at 2 mm min^{-1} . The tensile data were taken from the average value of 5 samples. The OM samples were used to measure the hardness after the OM experiments were performed. The Vickers microhardness was measured with a load of 100 g maintained for a loading time of 10 seconds using a Huayin type HV-1000A apparatus. For the as-cast sample, a total of ten points was randomly selected in the test plane. For the SD and HT samples, a total of ten points was randomly selected in the outer and inner areas, respectively. The maximum and minimum values were removed when calculating the average value and standard deviation. The sampling position is demonstrated in Figure 2.

III. RESULTS AND DISCUSSION

A. The Original Microstructure and Texture

The original microstructure of the LPDC A356 aluminum alloy is shown in Figures 3(a) and (b), and the black area in Figure 3(b) shows the unindexed eutectic Si particles. Figures 3(a) and (b) show that the microstructure of the LPDC A356 alloy is a typical dendritic structure. The A356 aluminum alloy is a hypereutectic alloy. During the solidification process, the α -Al dendrites precipitated first. Next, the Al-Si

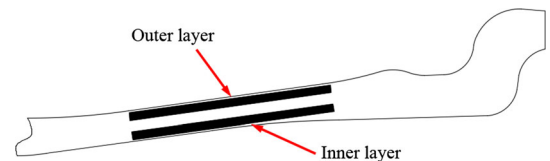


Fig. 2—Schematic diagram of sampling position.

eutectic crystals occurred in the dendritic arms, and the strengthening phases Mg_2Si precipitated in the cooling process.^[2] However, it was difficult to observe the Mg_2Si phase in the OM due to its low fraction and small size. Figure 3(a) also shows the morphologies of the eutectic Si observed in SEM; it is clear that the shapes of the as-cast eutectic Si are basically point, strip, or wormlike. The average MD is $1.45 (\pm 0.45) \text{ um}$ and the average R is $1.53 (\pm 0.5)$.

Figure 3(c) shows the misorientation angle distribution of the grain boundaries of the LPDC A356 aluminum alloy. It is obvious that the original grain boundaries mainly consisted of high-angle grain boundaries which accounted for approximately 70 pct, which are similar to the results reported by Abib *et al.*^[18] Figure 3(d) shows the ODF section diagram of the as-cast A356 aluminum alloy microstructure at $\varphi_2 = 0 \text{ deg}$ and $\varphi_2 = 45 \text{ deg}$, and the positions of the dominant texture components are shown in Table II. As shown in Figure 3(d), the initial as-cast microstructure had the features of type A_1 , A_2 , and brass R textures with some other weak textures randomly distributed.

B. Microstructural Evolution

The microstructures and morphologies of the eutectic Si particles of the outer layer and inner layer of the SD and HT samples are shown in Figure 4. As shown in the figure, there is a deformation gradient at the rim in the

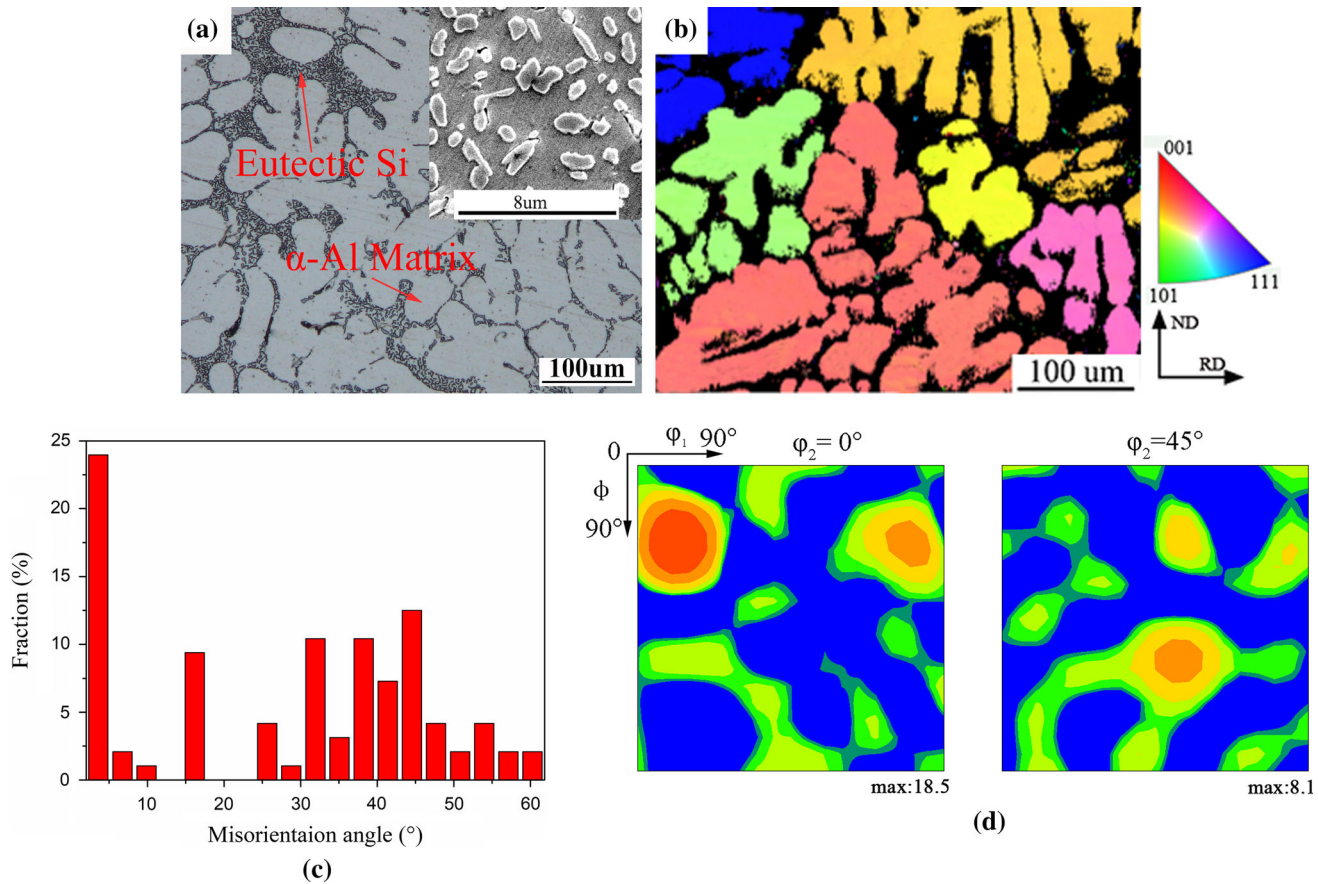


Fig. 3—The as-cast A356 aluminum alloy: (a, b) microstructure, (c) misorientation angle distribution, (d) ODF sections at ϕ_2 (0, 45 deg).

Table II. Euler Angles of Major Texture Components

Notation	Euler Angles (Deg)		
	ϕ_1	ϕ	ϕ_2
A ₁	15	25	0
A ₂	81	25	0
B	60	30	45
C	45	45	45
Brass R	0/60	55	45
Rotated cube	45	0	0
Goss	90	90	45

spinning process. The deformation in the outer layer was the largest, and the deformation in the inner layer near the die was much smaller than that in the outer layer. Figure 4(a) shows that the original as-cast microstructure had disappeared after the spinning processing, and the microstructure near the rollers presents a fiber streamline distribution, showing an obvious directionality. The grains were elongated, broken, refined, and arranged more closely under the action of the spinning stress, which is a typical spinning structure.^[7] As shown in Figure 4(b), the inner layer material also underwent severe plastic deformation, and the dendrite structure was compressed and elongated with

the generation of the fibrous structure. However, the streamline in the inner layer was not as obvious as that in the outer layer because the material flow in the inner region was blocked due to the frictional resistance between the die and the material, a similar phenomenon was reported by Shan *et al.*^[19] Figures 4(c) and (d) show the microstructure of HT sample. There were no obvious macroscopic changes compared with the SD microstructure, which is a sign of recovery.

As shown in Figures 4(a) through (d), the morphologies and dimensions of the eutectic Si particles changed significantly after heat treatment. Figure 5 presents the average value of MD and R of the eutectic Si in different layers and processing states. As shown in Figure 5(a), the MD of the SD eutectic Si particles slightly decreased after hot spinning compared with that of the as-cast state, but MD increased after heat treatment for both the outer and inner layer compared with that of the SD state. Due to the difference in elastic constants and deformation behavior between the eutectic Si particles and the α -Al matrix, the large plastic deformation under the action of the spinning stress led to a large mechanical strain at the interface, which caused the relatively brittle eutectic Si particles to be broken, thus reducing the size.^[20,21] According to the Ostwald mechanism,^[22] the solution treatment can accelerate the self-diffusion or mutual diffusion of Si *via* increasing the diffusion coefficient that leads to the aggregation of Si elements at

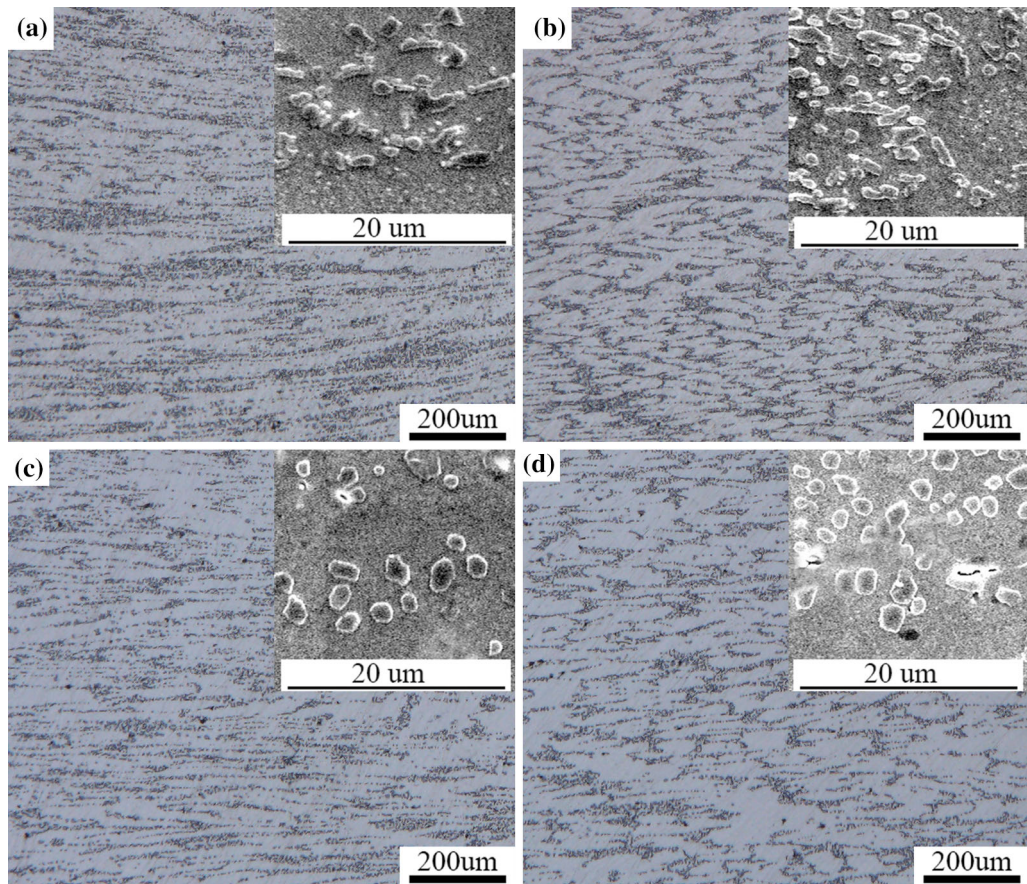


Fig. 4—Microstructure by OM and SEM: (a) SD-outer layer, (b) SD-inner layer, (c) HT-outer layer, (d) HT-inner layer.

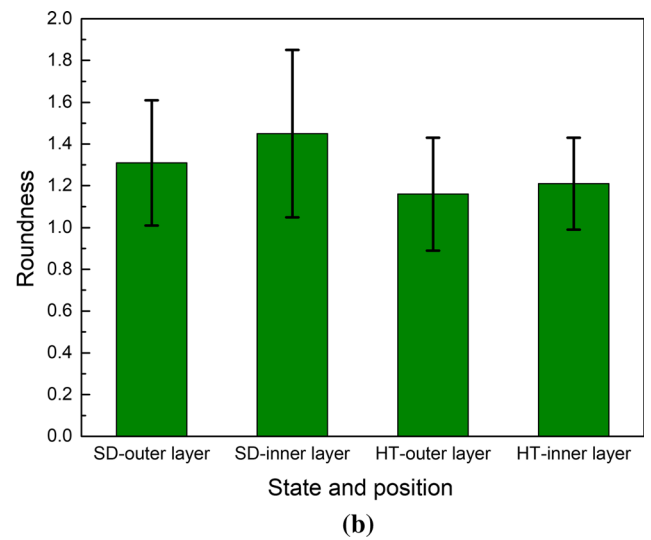
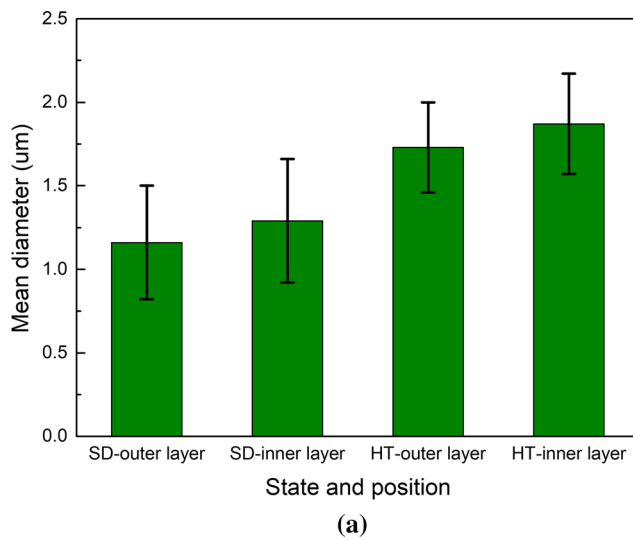


Fig. 5—Average values: (a) MD, (b) R.

the Si-Al interface, so the diameter of Si increased. As shown in Figure 5(b), R decreased slightly after hot spinning compared with that in the as-cast state, but decreased significantly after heat treatment. The

decrease in the value of R after the heat treatment was mainly caused by the thermal-activated spheroidization of the eutectic Si particles, this behavior is similar to that reported by Ogris *et al.* and Birol.^[23,24]

C. Texture Evolution

Figure 6 shows the orientation image maps of the outer layer and inner layer material in the SD and HT samples. The black points in the figure are the unindexed eutectic Si particles, and a similar experimental phenomenon has been reported by Bhaskar and Surappa.^[25] The plastic strain states of the inner and outer layers were obviously different due to the different stress states of these two regions during the spinning process, and thus different grain orientations formed, as shown in Figures 6(a) and (b). Aluminum alloys are metals with high stacking fault energy, and the width of the extended dislocation is narrow. In the process of thermal deformation, the dislocations are easy to cross slip and climb to generate dynamic recovery, so the deformation energy is not easy to accumulate, which makes it difficult to reach the critical state of dynamic recrystallization. Moreover, the recrystallization grains had not been observed in Figures 6(a) and (b), which indicated that the dynamic recovery of material occurred in the process of hot spinning. As shown in Figures 6(c) and (d), after heat treatment, there were isoaxial recrystallization grains in the outer layer, while the inner material did not recrystallize. The deformation energy is the driving force for recrystallization.^[26] The outer material that underwent a larger deformation accumulated more deformation energy than the inner layer material, so it was easier to reach the critical condition of recrystallization under the action of thermal activation. However, the material was not fully recrystallized even in the outer layer material; this is probably because the large amount of eutectic Si

particles increased the activation energy of the alloy and hindered recrystallization nucleation and growth, thus delaying the recrystallization process. As a result, the deformation energy was released through recovery before recrystallization, and the remaining deformation energy was not enough to cause recrystallization. Therefore, during the heat treatment process, the crystal orientation of the inner material was changed by static recovery.

Figure 7 is the ODF section diagram of the outer layer and inner layer of the SD and HT samples at $\varphi_2 = 0$ deg and $\varphi_2 = 45$ deg. As demonstrated in Figures 7(a) and (b), the original as-cast texture had basically disappeared after the hot spinning deformation, and some strong new textures occurred. In the outer layer of the rim, there were mainly strong rotated cube and brass R textures, while in the inner layer of the rim, there were mainly strong type C, brass R and weak Goss textures. The inhomogeneity of deformation between the outer layer and inner layer resulted in the difference in texture types. Figures 7(c) and (d) show that the heat treatment had a significant impact on the transformation of the spinning textures. After the heat treatment, some components of the spinning textures disappeared, and some components strengthened or weakened. In the outer layer, the rotated cube and brass R type textures disappeared, and a strong Goss texture formed. The weak texture component near $\varphi_2 = 60$ deg, $\varphi = 30$ deg, $\varphi_2 = 45$ deg significantly strengthened, so a strong type B texture occurred. In the inner layer, most of the texture components disappeared or weakened; only the type C texture remained, and some weak new texture components occurred. The recovery and

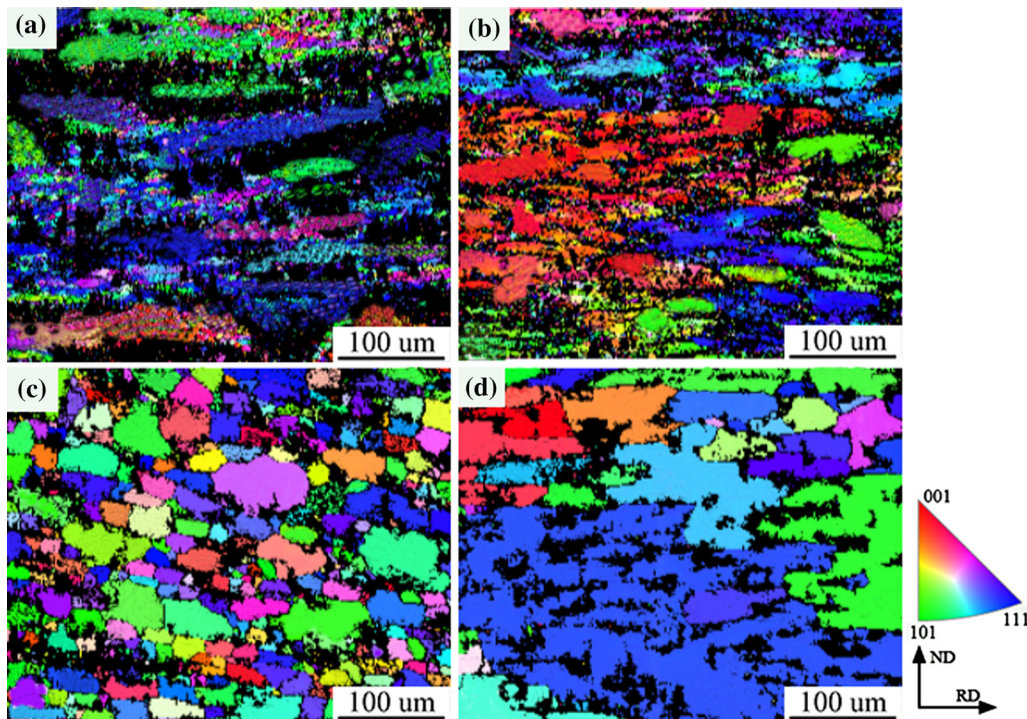


Fig. 6—Orientation image maps: (a) SD-outer layer, (b) SD-inner layer, (c) HT-outer layer, (d) HT-inner layer.

recrystallization in the process of heat treatment gave rise to the transformation of the deformed textures.

The distribution of the misorientation angle and the evolution of low-angle grain boundaries (LAGBs) and high-angle grain boundaries (HAGBs) of the outer layer and inner layer material at different states are shown in Figure 8. The SD samples were dominated by LAGBs, and the fraction of LAGBs for the inner and outer layers were 54.8 and 80 pct, respectively. When metals that have a high stacking fault energy and slip as their main deformation mechanism are deforming, the dislocations

group into high-density configurations due to interactions among the dislocations; dislocation entanglement occurs, and LAGBs form.^[27] After heat treatment, the fraction of LAGBs decreased rapidly, that of HAGBs increased significantly, and the proportion of HAGBs in the inner layer was higher than that in the outer layer. After metal recovery, the dislocation is not uniformly dispersed in the metal, but aggregated during the deformation process to form a cell-wall microstructure. The dislocations entangled to form LAGBs at high temperatures, and then formed a subcrystalline

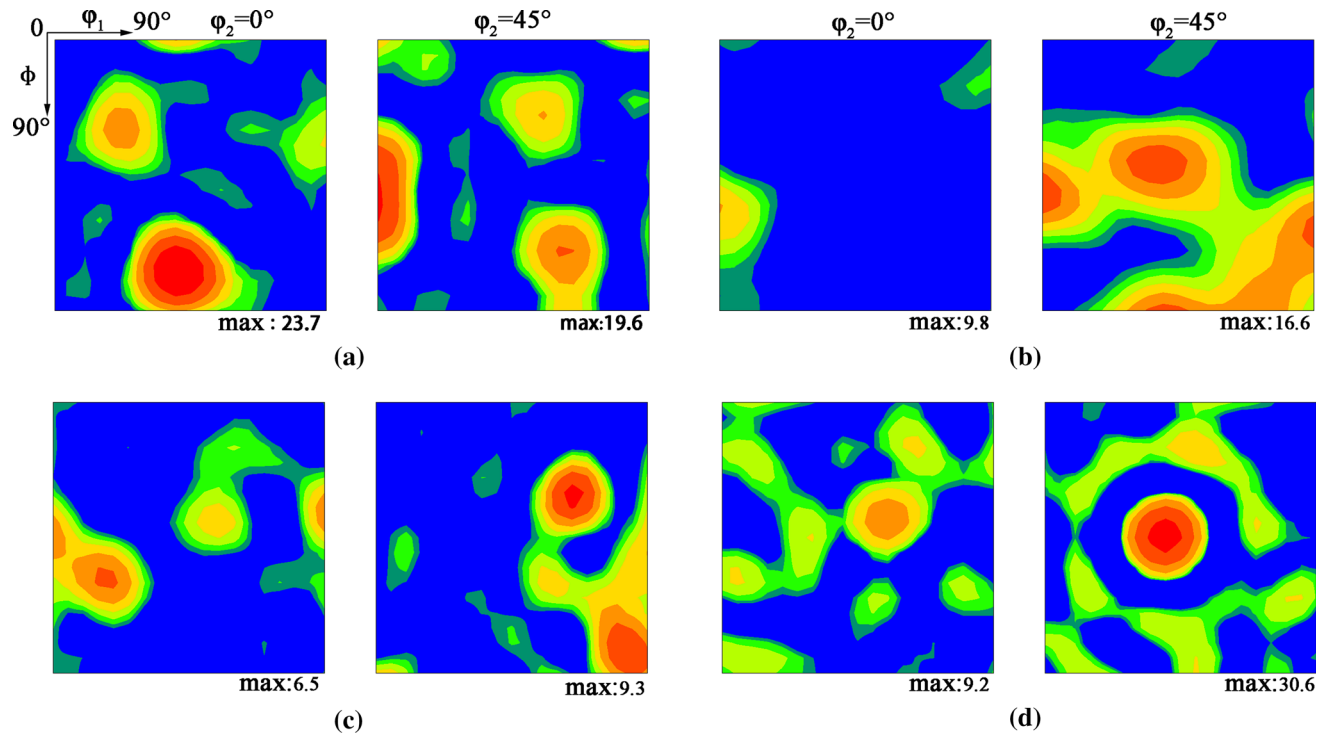


Fig. 7—ODF sections at $\phi_2 = 0$ and 45 deg: (a) SD-outer layer, (b) SD-inner layer, (c) HT-outer layer, and (d) HT-inner layer.

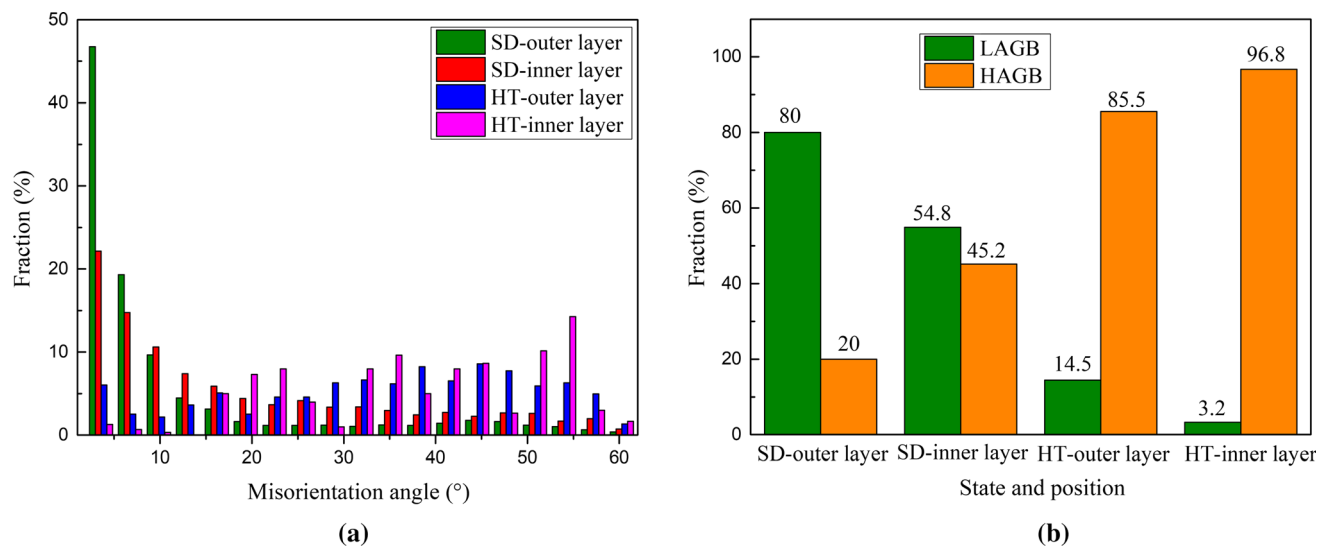


Fig. 8—(a) The misorientation angle distribution, (b) the evolution of LAGB and HAGB.

structure. With the movement of dislocations, the dislocation continued to entangle and aggregate in the LAGBs, so that the misorientation angle of the subgrain boundaries gradually became larger. Hence, the HAGBs and recrystallized grains formed.

D. Mechanical Properties

1. Hardness

The average values of hardness in different regions and different processing states are summarized in Table III. The hardness decreased substantially after spinning in comparison with the as-cast specimen, and that of the outer layer was slightly lower than that of the inner layer. However, the hardness of SD samples increased significantly after the heat treatment. The mechanical properties of Al-7Si-Mg alloy are largely determined by the morphology and dimension of the α -Al matrix and the eutectic Si particles.^[28,29] It is commonly accepted that in the Al-7Si alloy, eutectic Si is the predominant factor that resists local plastic deformation.^[6] Hot spinning resulted in a decrease in the size of α -Al dendrite spacing and eutectic Si particles. The ability of the granular Si particles distributed on the matrix to resist plastic deformation was lower than that of vermicular or strip-shaped Si particles in the as-cast state, leading to a decrease in hardness. The slight difference in hardness between the inner and outer layers was caused by the uneven deformation. During the heat treatment process, the solute Mg and Si atoms clustered and precipitated in Gunier–Preston (GP-Mg₂Si₃Al₆) zones along the $\langle 100 \rangle$ direction. A dissolved rod/plate-shaped equilibrium Mg₂Si FCC phase was finally precipitated owing to minor atomic rearrangement in the matrix. The precipitate and its growth promoted an increase in hardness.^[30,31] The increase in the size of eutectic Si is another factor that contributes to the increase in hardness.

2. Tensile Properties

The yield strength (YS), ultimate tensile strength (UTS) and elongation of the SD and HT samples in the inner and outer layers are listed in Table III. As presented in the table, despite the poor mechanical properties, the strength and elongation of the as-cast alloy were substantially improved by spinning. Specifically, the UTS increased from 217 to 259 MPa and 250 MPa for the outer layer and inner layer. The elongation increased from 13 to 21 pct for the layer

and inner layers. As described in Section III–B, the grains in the rim were refined by hot spinning. According to the Hall–Petch formula, the refined grains can significantly enhance the strength of the alloy.^[32,33] At the same time, a good deal of dislocations occurred in the process of spinning. In the process of tension, the motion of dislocations was hindered by the secondary precipitate particles and solute atoms in the alloy; thus, the dislocations themselves tangled. Hence, a larger force was needed to activate the movement of the dislocations, so a higher strength was achieved.^[6] The fracture path preferentially goes through the casting defects, resulting in poorer mechanical properties, especially poor ductility. The elimination of porosity by spinning is the main factor for the enhancement of ductility, and plays an important role in the increase of UTS. As shown in the Table III, the UTS after heat treatment was further improved to 291 and 284 MPa of the outer layer and inner layer material compared with the SD samples, but the elongation decreased. After heat treatment, the presence of the better spheroidized eutectic Si particles retarded crack nucleation as the stress concentration effect on the particles was reduced. Accordingly, the stress or strain needed to crack an HT specimen was much higher than that of an SD specimen. On the other hand, the precipitated nanometer acicular Mg₂Si also increased the tensile strength, but the brittle precipitated phase resulted in the reduction of α -Al matrix deformation, thus decreasing the elongation.^[34]

The texture developed during deformation or heat treatment is a key factor that can affect the YS. To investigate the effect of the textures on YS, the average value and distribution of the Schmid Factor (SF) for the SD and HT samples were calculated from the EBSD data, as shown in Figure 9. The higher the SF, the easier for the orientated grains to slip, or *vice versa*.^[34] It can be seen from Figure 9 that the average value of SF after heat treatment is lower than that in the spinning state, and the average value of SF in the outer layer is lower than that in the inner layer in both states. The higher SF indicates that the slip system of the material is easier to activate, which means that the stress is lower when plastic deformation occurs. Decreasing strength by increasing SF has been reported elsewhere.^[15,35,36] The change of SF in Figure 9 is consistent with the variation of YS in Table III. Hence, it can be concluded that the new textures that occurred in the heat treatment process had a strengthening effect on the studied material.

Table III. Mechanical Properties of A356 at Various States and Regions

Sample	Microhardness (Hv _{0.1})	Yield Strength (MPa)	UTS (MPa)	Elongation (Pct)
As-Cast	66.7 (± 3.0)	155.6 (± 5.0)	216.7 (± 3.2)	13.0 (± 0.5)
SD-Outer Layer	50.2 (± 1.7)	198.9 (± 3.0)	258.8 (± 2.7)	21.4 (± 1.0)
SD-Inner Layer	53.4 (± 2.1)	185.4 (± 4.0)	250.2 (± 2.3)	20.7 (± 0.5)
HT-Outer Layer	86.3 (± 2.0)	247.7 (± 3.2)	290.6 (± 2.0)	15.3 (± 0.7)
HT-Inner Layer	90.7 (± 2.3)	231.2 (± 3.0)	283.5 (± 2.0)	15.0 (± 1.0)

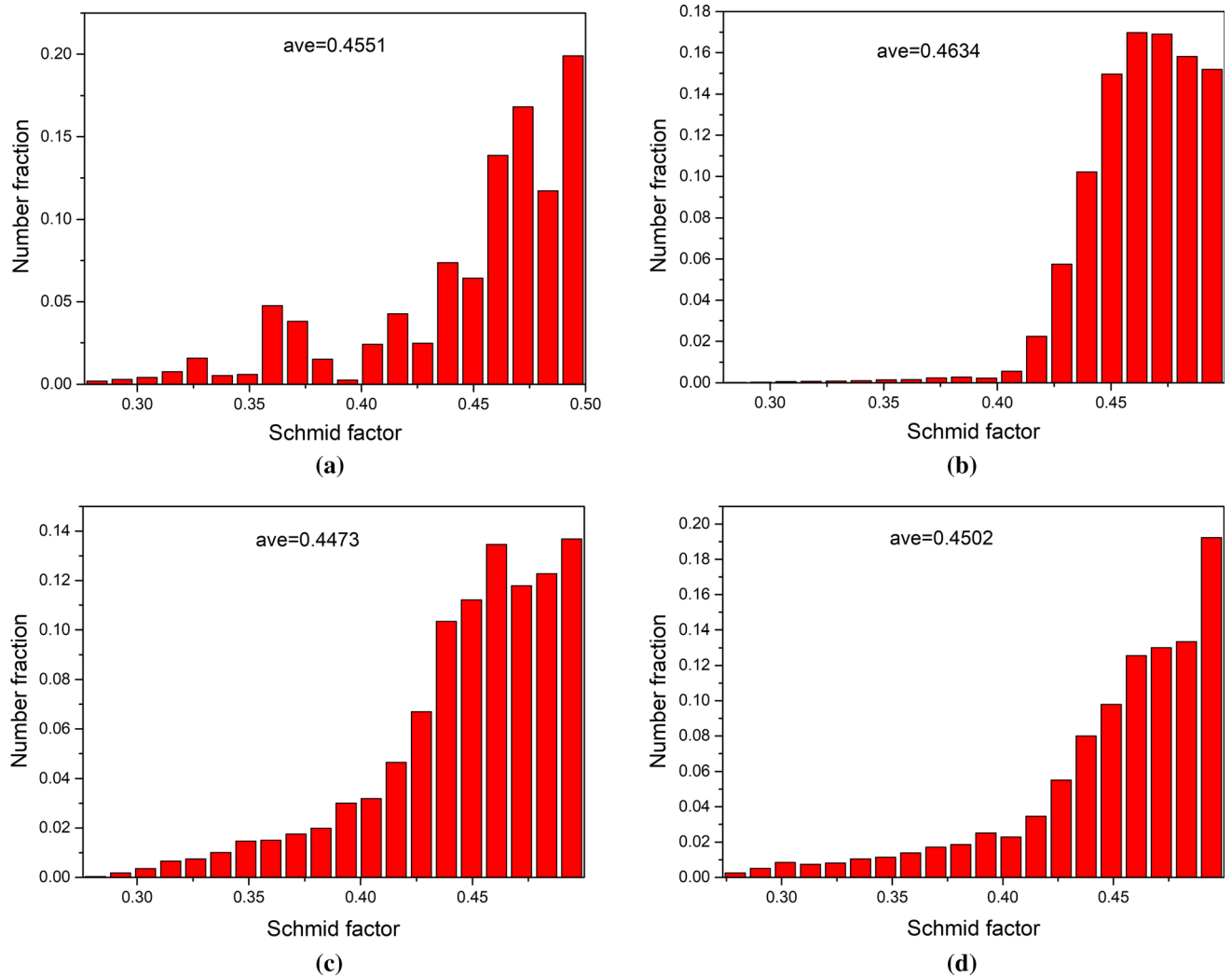


Fig. 9—SF distribution for SD and HT samples: (a) SD-outer layer, (b) SD-inner layer, (c) HT-outer layer, (d) HT-inner layer.

IV. CONCLUSIONS

The effects of hot spinning and heat treatment on the microstructure, texture and mechanical properties of A356 wheel hubs were investigated in the present study, and the following conclusions can be made:

1. The microstructure of the as-cast A356 aluminum alloy was a dendritic structure, which showed the texture characteristics of type A_1 , A_2 and brass R. The grain boundaries were dominated by HAGBs.
2. Hot spinning elongated and refined the as-cast microstructure, forming a streamlined microstructure. Due to the uneven deformation between the outer layer and inner layer, the streamline in the inner layer was not as obvious as that of the outer layer. There was an increase in MD and a decrease in R of the eutectic Si particles after heat treatment.
3. After hot spinning, the original as-cast texture had basically disappeared, and the strong rotated cube

and brass R textures appeared in the outer layer of the rim, while the strong type C, brass R and weak Goss textures mainly occurred in the inner layer of the rim. The grain boundaries in the SD sample were dominated by LAGBs. After heat treatment, some of the spinning texture components disappeared, some were strengthened or weakened, and strong Goss, type B and C textures occurred. LAGBs gradually transformed to HAGBs because of the static recovery and recrystallization during the heat treatment process.

4. Hot spinning decreased the hardness of the material, but the subsequent heat treatment significantly increased it. Both hot spinning and heat treatment could greatly improve the strength of the A356 alloy, but heat treatment reduced the elongation. The evolution of textures developed in the processes of hot spinning and heat treatment had an effect on YS.

ACKNOWLEDGMENTS

The authors appreciate financial support from the Natural Science Foundation of China under Grant 51275533, the State Key Laboratory of High-Performance Complex Manufacturing (Contract No. zzyjk-t2013-10B), Central South University, China.

REFERENCES

1. W.M. Jiang, Z.T. Fan, D.J. Liu, D.F. Liao, X.P. Dong, and X.M. Zong: *Mater. Sci. Eng. A*, 2013, vol. 560, pp. 396–403.
2. B. Milkereit, H. Frock, C. Schick, and O. Kessler: *Trans. Nonferrous Met. Soc. China*, 2014, vol. 24, pp. 2025–33.
3. Y.J. Zhang, N.H. Ma, Y.K. Le, S.C. Li, and H.W. Wang: *Mater. Lett.*, 2005, vol. 59, pp. 2174–77.
4. S.C. Wang, C. Cai, K.H. Zheng, and W.J. Qi: *China Foundry*, 2013, vol. 10, pp. 299–303.
5. M.J. Roy and D.M. Maijer: *J. Mater. Process. Technol.*, 2015, vol. 226, pp. 188–204.
6. X.Y. Wu, H.R. Zhang, H.L. Chen, L.N. Jia, and H. Zhang: *China Foundry*, 2017, vol. 14, pp. 138–44.
7. Y.C. Cheng, C.K. Lin, A.H. Tan, S.Y. Hsu, and S.L. Lee: *J. Mater. Eng. Perform.*, 2012, vol. 21, pp. 1873–78.
8. W.M. Zhao, X.F. Jia, Z.F. Wang, Z.G. Yin, and G.Y. Xiong: *Adv. Mater. Res.*, 2011, vols. 189–193, pp. 4014–17.
9. Y.C. Cheng, C.K. Lin, A.H. Tan, J.C. Lin, and S.L. Lee: *Mater. Manuf. Process.*, 2010, vol. 25, pp. 689–95.
10. B. Dang, Y.B. Li, F. Liu, Q. Zuo, and M.C. Liu: *Mater. Des.*, 2014, vol. 57, pp. 73–78.
11. R. Gupta, A. Sharma, U. Pandel, and L. Ratke: *Int. J. Cast. Metals Res.*, 2017, vol. 30, pp. 283–92.
12. M. Zhu, Z.Y. Jian, G.C. Yang, and Y.H. Zhou: *Mater. Des.*, 2012, vol. 36, pp. 243–49.
13. V.H. Carneiro, H. Puga, and J. Meireles: *Mater. Sci. Eng. A*, 2018, vol. 729, pp. 1–8.
14. J.H. Peng, X.L. Tang, J.T. He, and D.Y. Xu: *Trans. Nonferrous Met. Soc. China*, 2011, vol. 21, pp. 1950–56.
15. M. Howeyze, A.R. Eivani, H. Arabi, and H.R. Jafarian: *Mater. Sci. Eng. A*, 2018, vol. 732, pp. 120–28.
16. A. Tajir, Y. Uematsu, T. Kakiuchi, Y. Tozaki, Y. Suzuki, and A. Afrinaldi: *Int. J. Fatigue*, 2015, vol. 80, pp. 192–202.
17. S.S. Zhao, X.P. Lin, Y. Dong, Y. Niu, D. Xu, and H. Sun: *Mater. Sci. Eng. A*, 2018, vol. 729, pp. 300–09.
18. K. Abib, J.A.M. Balanos, B. Alili, and D. Bradai: *Mater. Charact.*, 2016, vol. 112, pp. 252–58.
19. D.B. Shan, G.P. Yang, and W.C. Xu: *J. Mater. Process. Technol.*, 2009, vol. 209, pp. 5713–19.
20. M.G. Mueller, M. Fornabaio, G. Zagar, and A. Mortensen: *Acta Mater.*, 2016, vol. 105, pp. 165–75.
21. U. Patakham and C. Limmaneevichit: *J. Alloys Compd.*, 2014, vol. 616, pp. 198–207.
22. L. Yang, Y.B. Li, B. Dang, H.B. Lu, and F. Liu: *Trans. Nonferrous Met. Soc. China*, 2015, vol. 25, pp. 3189–96.
23. E. Ogris, A. Wahlen, H. Luchinger, and P.J. Uggowitzer: *J. Light Met.*, 2002, vol. 2, pp. 263–269.
24. Y. Birol: *Mater. Sci. Eng. A.*, 2013, vol. 559, pp. 394–400.
25. M.S. Bhaskar and M.K. Surappa: *Trans. Indian Inst. Met.*, 2019, vol. 72, pp. 849–57.
26. W.C. Liu, C.S. Man, D. Raabe, and J.G. Morris: *Scr. Mater.*, 2005, vol. 53, pp. 1273–77.
27. Y.C. Lin, X.Y. Wu, X.M. Chen, J. Chen, D.X. Wen, J.L. Zhang, and L.T. Li: *J. Alloys Compd.*, 2015, vol. 640, pp. 101–13.
28. Y. Birol: *J. Alloys Compd.*, 2009, vol. 484, pp. 164–67.
29. J.B. Yu, Z.M. Ren, W.L. Ren, K. Deng, and Y.B. Zhong: *Acta Metall. Sin. Engl. Lett.*, 2009, vol. 22, pp. 191–96.
30. G. Sha, H. Moller, W.E. Stumpf, J.H. Xia, G. Govender, and S.P. Ringer: *Acta Mater.*, 2012, vol. 60, pp. 692–701.
31. K. Buchanan, K. Colas, J. Ribis, A. Lopea, and J. Garnier: *Acta Mater.*, 2017, vol. 132, pp. 209–21.
32. Y.B. Chun, S.H. Ahn, D.H. Shin, and S.K. Hwang: *Mater. Sci. Eng. A.*, 2009, vol. 508, pp. 253–58.
33. P. Luo, D.T. McDonald, S.M. Zhu, S. Palanisamy, M.S. Dargusch, and K. Xia: *Mater. Sci. Eng. A.*, 2012, vol. 538, pp. 252–58.
34. O.R. Myhr, O.S. Hopperstad, and T. Borvik: *Metall. Mater. Trans. A*, 2018, vol. 49A, pp. 3592–3609.
35. S. Biroasca, F. Di Gioacchino, S. Stekovic, and M. Hardy: *Acta Mater.*, 2014, vol. 74, pp. 110–24.
36. S.M. Fatemi, A. Zarei-Hanzaki, and J.M. Cabrera: *Metall. Mater. Trans. A*, 2017, vol. 48A, pp. 2563–73.

Publisher's Note Springer Nature remains neutral with regard to jurisdictional claims in published maps and institutional affiliations.